Electronic Raman and infrared spectra of acceptors in isotopically controlled diamonds

Hyunjung Kim, R. Vogelgesang, A. K. Ramdas, and S. Rodriguez
Department of Physics, Purdue University, West Lafayette, Indiana 47907-1396

M. Grimsditch
Argonne National Laboratory, Argonne, Illinois 60439

T. R. Anthony
General Electric Company Corporate Research and Development, Schenectady, New York 12309
(Received 3 February 1998)

The Lyman spectrum of substitutional boron acceptors in diamonds with natural composition and that in a ^{13}C diamond exhibit remarkably similar features, but shifted to higher energies in the latter by 0.4–1.5 meV. Additional lines appear when the spectra are recorded as a function of temperature, indicating the thermal population of a level $\Delta' \sim 2$ meV above the ground state; this can be interpreted as the spin-orbit splitting of the $1s$ acceptor ground state into $1s(p_{3/2})$ and $1s(p_{1/2})$, the latter located Δ' above the former. The Raman-allowed $1s(p_{3/2}) \rightarrow 1s(p_{1/2})$ electronic transition is directly observed at 2.07(1) and 2.01(1) meV in the Raman spectrum of natural and ^{13}C diamond, respectively. Polarization features of the Δ' Raman line reveal that it is predominantly Γ_5 in character, as predicted by a theoretical calculation formulated in terms of the known values of Luttinger parameters. The theoretical expression for the Raman cross section for Δ' enables the acceptor concentration to be deduced from an intercomparison of the intensity of the Δ' line and that of the zone-center optical phonon. The presence of boron acceptors produces a quasicontinuous absorption spectrum in the range of the optical phonon branch, flanked by a sharp feature at the zone-center optical phonon frequency; their appearance can be attributed to the partial breakdown of the translational symmetry and the activation of otherwise inactive vibrations. [S0163-1829(98)03624-8]

I. INTRODUCTION

Diamonds have been classified as type I if their infrared absorption spectra exhibit impurity dependent, i.e., *extrinsic* features in the 6.5–15 μm range; the relatively rarer type II specimens are, in contrast, transparent in this region.[1] Both types display *intrinsic* absorption bands in the 2.5–6.5 μm range, now known to be due to multiphonon excitations.[2] Kaiser and Bond[3] reported the striking observation that the extrinsic infrared absorption bands arise from the presence of nitrogen in type I diamonds whereas type II diamonds are nitrogen-free. Custers[4] made the startling discovery that there are extremely rare specimens of type II diamonds which are highly conducting, some with resistivities as low as 25 Ω cm, whereas type I and II specimens typically exhibit resistivities well in excess of 10^{16} Ω cm. The low resistivity diamonds have been designated as type IIb whereas the nitrogen-free, high resistivity specimens are classified as type IIa. On the basis of Hall effect studies, Austin and Wolfe[5] and Wedepohl[6] showed that type IIb diamonds are p type, acceptor concentrations as high as 5×10^{16} cm^{-3} being encountered in their studies. Further, the infrared spectra of type IIb diamonds exhibit Lyman transitions characteristic of the bound states of the acceptor-bound holes.[5–9]

Even after the successful synthesis of diamond with the high-pressure-high-temperature technique[10] (HPHT) and with chemical vapor deposition (CVD),[10,11] only p-type doping with substitutional group III boron impurities has been successful.[12] Boron-doped diamonds are bluish to distinctly blue in color as a result of the absorption in the red due to the photo-ionization continuum of holes bound to boron acceptors, the intensely blue Hope diamond being a striking example. The physics of the bound states of acceptors, well documented for Si and Ge,[13] needs to be fully explored for diamond.

Our infrared studies on the Lyman spectra of neutral boron acceptors in natural type IIb specimens, a man-made boron-doped sample with natural carbon composition, i.e., $^{12}C_{0.989}{}^{13}C_{0.011}$, and a boron-doped ^{13}C diamond have revealed *a remarkable example of ''central cell'' corrections for the same substitutional acceptor but located in a host differing merely in its isotopic composition*. We have also discovered the Raman transition between the spin-orbit split ground states of the boron acceptor in all the specimens; once again, an isotope-related, small but spectroscopically accessible difference is manifested. We have published short reports[14,15] of these findings. In the present paper we give a complete account of these investigations along with the underlying theory.

II. EXPERIMENTAL PROCEDURE

Two type IIb specimens of natural diamond as well as a boron-doped diamond of natural composition and a boron-doped ^{13}C diamond, grown by CVD followed by the HPHT technique, were studied in the present investigation. The boron doping of the man-made diamonds was accomplished by adding 99.999% pure amorphous, submicrometer, boron powder[16] to the diamond growth cell mixture of powdered 97% Fe-3% Al metal solvent, and a feedstock of CVD dia-

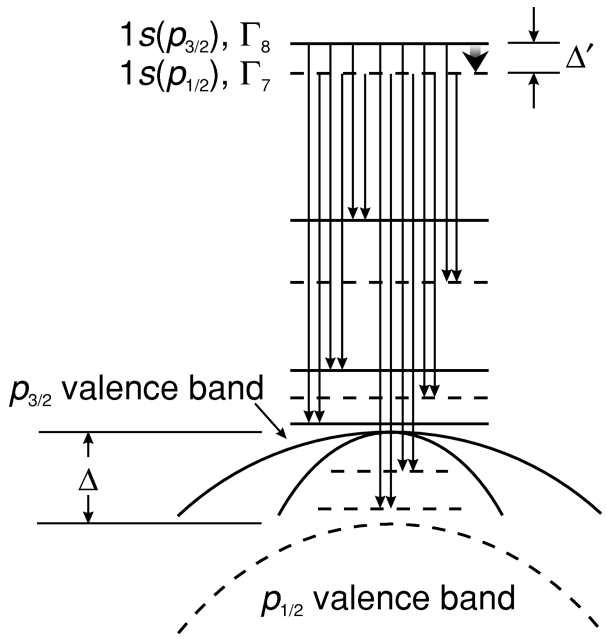

FIG. 1. Energy levels of a hole bound to a substitutional boron acceptor shown schematically. The diagram also shows the Lyman transitions from the ground state associated with the $p_{3/2}$ valence band (solid line) as well as those associated with the $p_{1/2}$ valence band (dashed line). Δ is the energy difference between the maxima of the two bands and Δ' that between the two ground states, associated with the $p_{3/2}$ and the $p_{1/2}$ valence bands, respectively.

mond powder having natural or ^{13}C composition. Several natural type IIa and a ^{13}C type IIa (nominally boron-free) specimens were also investigated for comparison.

The infrared transmission of the diamond specimens was measured with a BOMEM DA3 Fourier transform spectrometer[17] and a cooled mercury cadmium telluride detector[18] operating at 77 K. A resolution of 1.0 cm^{-1} proved adequate for recording the spectra in view of the half-widths of the excitation lines. The Raman spectra were recorded on a Jobin Yvon, charge-coupled-device- (CCD) based, multichannel triple spectrometer[19] or on a Spex 14018 double (triple) spectrometer[19] equipped with a RCA photomultiplier tube (type C31034A) and standard photon-counting electronics. Several lines of an Ar^+ laser (Coherent Model 10),[20] a Kr^+ laser (Spectra Physics Model 171),[21] and a He-Cd laser (Omnichrome 2074) (Ref. 22) were used to excite the Raman spectra. Both infrared and Raman spectra were studied as a function of temperature using variable temperature cryostats.[23]

III. ELECTRONIC TRANSITIONS OF ACCEPTOR-BOUND HOLES: GENERAL CONSIDERATIONS

As is well known,[13] substitutional group III boron, replacing a group IV host atom in an elemental semiconductor, is an acceptor with a hole bound to it at sufficiently low temperatures; the bound states of the hole are shown schematically in Fig. 1. In the effective mass theory (EMT),[24] including spin-orbit effects, these states are associated with the $p_{3/2}(\Gamma_8^+)$ and $p_{1/2}(\Gamma_7^+)$ valence band maxima located at the zone center. The wave functions of the bound states are products of hydrogenic envelope functions and Bloch functions characteristic of the valence band maxima. Consistent with the $\overline{T}_d$ symmetry of the substitutional acceptor, the bound states are characterized by Γ_6, Γ_7, or Γ_8 symmetry. The $1s(p_{3/2})$ and $1s(p_{1/2})$ ground states have Γ_8 and Γ_7 symmetry, respectively. The binding energies of the *s*-like and *p*-like states are determined by the effective mass parameters, or equivalently by the Luttinger parameters,[25] and the dielectric constant of the host. In addition, the bound states might experience shifts originating in the departures from EMT, i.e., the so-called *''central cell'' corrections*.[13,26]

At the lowest temperature, the electric-dipole-allowed transitions from the $1s(\Gamma_8)$ to the excited *p* states, i.e., the Lyman lines, are observed for the boron acceptors in diamond in the range 2400–5500 cm^{-1} as absorption peaks;[5–9,14] as minima in the photoconductivity for phonon-assisted transitions occurring above the photoionization limit;[9,27] or as peaks due to the photothermal ionization from the excited states.[28] In Raman spectroscopy, being driven by nonvanishing ''transition'' polarizability, one can observe transitions only between even parity states;[29] this is also true for two-photon transitions.[30] For diamond, we have discovered the $1s(\Gamma_8)$ to $1s(\Gamma_7)$ transition to be discussed in Sec. V. Coherent anti-Stokes Raman scattering[31] is yet another spectroscopic technique in which the selection rules for the resonances observed are identical to those in Raman scattering and two-photon absorption spectroscopy. The ''two-electron transitions'' in the luminescence spectrum of donor-bound excitons in GaP[32] and in Ge,[33] the far infrared absorption spectra of a steady state population of donor- or acceptor-bound excitons in Si,[34] and the luminescence excitation spectroscopy of donor-acceptor pairs in GaP[35] are additional examples of spectroscopic phenomena in which the bound states of donors and/or acceptors have been observed and delineated.

The spin-orbit splitting of the valence band of diamond, i.e., the energy separation Δ between the $p_{3/2}(\Gamma_8^+)$ and the $p_{1/2}(\Gamma_7^+)$ valence band maxima, has been deduced by Rauch[36] on the basis of cyclotron resonance of holes; he detected the mm-wave cyclotron resonance of the light holes in the $p_{3/2}$ band as well as the holes in the $p_{1/2}$ band by selectively populating the respective bands employing light from a monochromator, magnetic fields being selected to achieve cyclotron resonance for the specific band. His measurements yielded $\Delta = 6$ meV. The corresponding spin-orbit splitting of the $1s$ ground states, Δ', need not be the same as shown by Lipari and Baldereschi for acceptors in Si.[37]

IV. LYMAN TRANSITIONS IN THE INFRARED

In Fig. 2, the absorption spectrum of a natural type IIb (D1) and of a type IIa (D18) diamond, recorded at 5 K, are compared in the spectral range 1800–6000 cm^{-1}. While both clearly display the same multiphonon features in the range 1800–2300 cm^{-1}, the type IIb specimen exhibits over 28 distinct and sharp excitation lines of varying linewidths ranging from ~ 5 to 44 cm^{-1}. These lines constitute the Lyman spectrum of the substitutional boron acceptors in diamond.[5–9,14,15,38,39] The inset shows the excitation lines of another natural type IIb (D2) specimen in the range 2750–2850 cm^{-1}. The boron concentration of D2 is clearly smaller

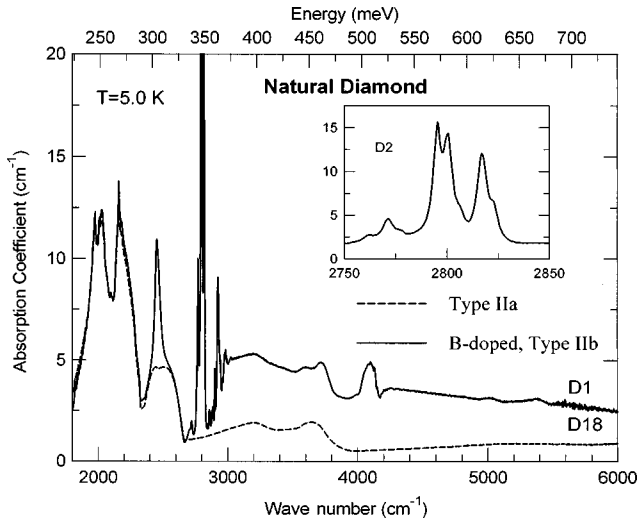

FIG. 2. The Lyman spectra of natural type IIa (D18) and of type IIb (D1) diamonds at temperature $T=5.0$ K. The inset shows the most intense electronic transitions in the range of 2750–2850 cm^{-1} for a natural type IIb (D2) specimen having a smaller boron concentration.

than that of D1,[40] allowing a clear observation of the intense lines. The photoionization continuum beginning $\sim 3000\ cm^{-1}$ extends well into the red and accounts for the characteristic blue color of type IIb diamonds. The broad absorption feature in the range 3600–4300 cm^{-1} is attributed to electronic transitions coupled with the ''defect-induced-first-order (DIFO), one-phonon density of states spectrum'' and that in the range 4800–5500 cm^{-1} to electronic transitions accompanied by the overtones and combinations of the DIFO. We will discuss these further in Sec. VI.

In a similar fashion, Fig. 3 shows the absorption spectrum of a single crystal ^{13}C, type IIa (D40) and of a type IIb

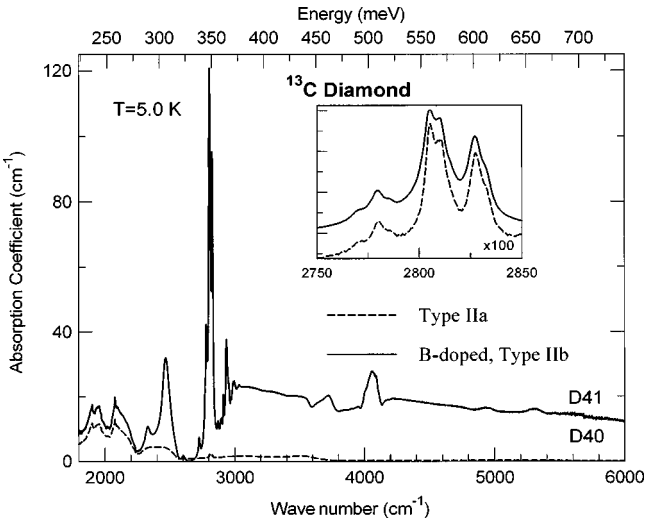

FIG. 3. The absorption spectrum of a ^{13}C nominally type IIa, and of a boron-doped diamond recorded at 5.0 K. The comparison between the spectra of the two specimens (the spectrum of type IIa enlarged 100 times) in the range of 2750–2850 cm^{-1} shown in the inset. The type IIa diamond here evidently was contaminated by boron during growth.

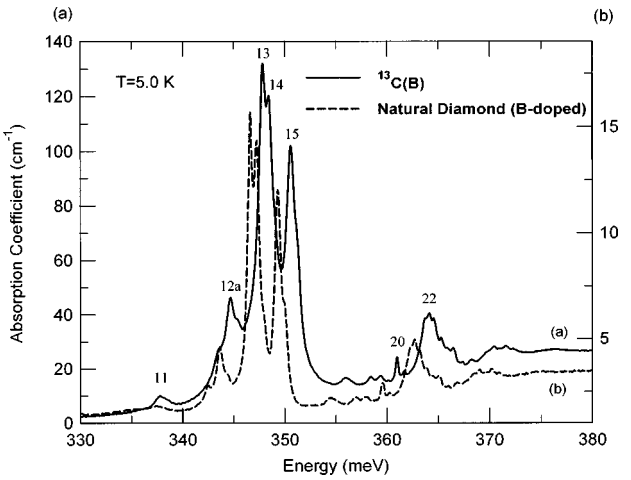

FIG. 4. Comparison of the excitation spectrum of a natural type IIb (D2) and a ^{13}C boron-doped diamond in the range 330–380 meV. The energies of the corresponding lines are given in Table I.

(boron-doped) (D41) diamond. The characteristic electronic excitations of the acceptor-bound holes in the type IIb diamond appear strikingly. Note that the shift of the underlying phonon feature in the ^{13}C specimen has revealed the weak electronic transition at 288.8 meV. This is the analog of the 289.8 meV line reported by Davies and Stedman for natural type IIb diamond.[27] The inset compares the absorption spectrum of the type IIb and that of the type IIa diamond, the latter magnified 100 times. It thus appears that the nominally boron-free type IIa diamond is not entirely free of boron (presumably introduced inadvertently during growth).

The comparison between a natural and a ^{13}C type IIb diamond is emphasized in Fig. 4 in the range of the sharp excitation lines. The spectra are remarkable in their exact correspondence even to the minutest detail. Further, they exhibit a unique feature: the corresponding lines of the ^{13}C diamond are *shifted to higher energies by increasing amounts*, from 0.4 to 1.5 meV, as can be seen from Table I. In contrast, the multiphonon features of the ^{13}C diamond are shifted to *lower* energies with respect to those in the natural diamond as is to be expected from the virtual crystal approximation (VCA) (scaling according to the inverse square root of the average isotopic mass of carbon, i.e., $\bar{M}^{-1/2}$). *This is a unique example of the ''central cell'' corrections to the binding energies of bound states of a substitutional acceptor (boron, in this case) being influenced by the isotopic composition of the host, over and above the chemical nature of the acceptor*.

TABLE I. Energies of the most prominent electronic transitions of boron acceptors in diamond (meV).

Line no.	Natural diamond	^{13}C diamond	Difference
11	337.38	337.76	0.38
12a	343.60	344.65	1.05
13	346.60	347.81	1.21
14	347.21	348.37	1.16
15	349.29	350.54	1.25
20	359.56	360.96	1.40
22	362.64	364.10	1.46

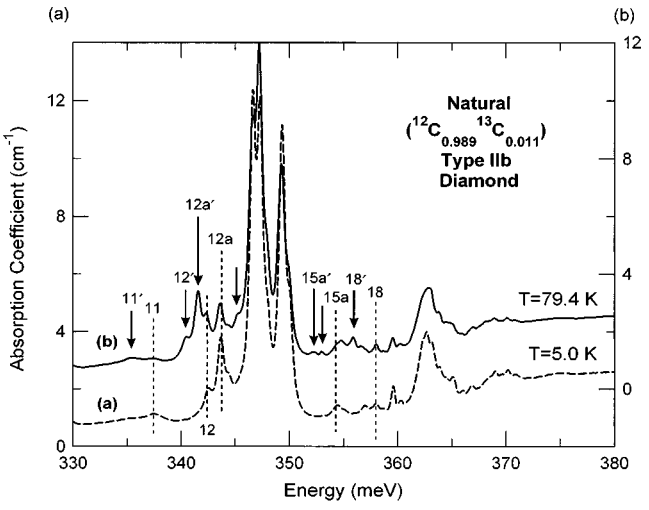

FIG. 5. The Lyman transitions of holes bound to boron acceptors in a natural diamond recorded at $T=79.4$ K and $T=5.0$ K. The arrows identify the new lines which appear at higher temperatures. Note the difference between the two lines labeled with the same number (unprimed and primed) is ~ 2 meV.

In order to account for the shift of the excitation spectrum of boron acceptors in ^{13}C diamond with respect to that in natural diamond, we have made preliminary estimates invoking several mechanisms consistent with the difference in their atomic volumes. The estimated change in the dielectric constant gives rise to negligible shifts ($\sim 10^{-3}$ to 10^{-4} meV) in the binding energies of the effective mass states. The changes in the Coulomb energy of the hole in the presence of the ionized acceptor yield a ground state shift no more than 10^{-2} meV for two approximations we considered: the charge of the ion was considered to be uniformly distributed over its volume in one and over its surface in the other. The contribution of the tetrahedral potential leads to shifts of no more than 0.2 meV. A preliminary analysis taking into account the position dependence of the dielectric constant also yielded negligible effects. Another mechanism[41] one could invoke views the self-energy of the states to arise from the electron-phonon coupling as discussed by Collins *et al.*[42] in the case of the indirect gap. This self-energy correction is proportional to the square of the amplitude of the lattice vibrations and hence varies as the inverse square root of the isotopic mass. Thus the difference of such a contribution between that in ^{13}C and in natural diamond is proportional to $[1-(\overline{M}_{\rm nat}/\overline{M}_{13})^{1/2}]$, where $\overline{M}_{\rm nat}$ and $\overline{M}_{13}$ are the corresponding average isotopic masses. The magnitude of this shift cannot be easily estimated since it would require knowledge of the temperature dependence of a specific electronic transition, say, for natural diamond. In the temperature range in which well resolved excitation lines have been observed, such shifts are negligible within 5 to 300 K.

The Lyman transitions in a natural type IIb diamond, recorded at 5.0 K and 79.4 K, respectively, are compared in Fig. 5. The arrows indicate new lines which appear as the temperature is raised, evidently due to the thermal population of an excited state lying close to the lowest $1s$ ground level. Indeed, in EMT, these are associated with the $p_{3/2}$ and $p_{1/2}$ valence bands, with the $1s(p_{1/2})$ hole ground state less tightly bound than the $1s(p_{3/2})$ hole ground state as shown schematically in Fig. 1. If the final state of two excitations originating in $1s(p_{3/2})$ and $1s(p_{1/2})$ is the same, the energy difference between them will yield Δ', the spin-orbit splitting of the $1s$ ground state. From a comparison of absorption spectra at 5.0 K and 79.4 K, it is possible to identify pairs of lines (one appearing in both spectra and the other only at the higher temperature) whose separations are very close. The pairs, $(11,11')$, $(12,12')$, $(12a,12a')$, $(15a,15a')$, $(18,18')$, all exhibit a separation close to 2 meV. This is a strong indication that this separation represents the spin-orbit splitting of the $1s$ ground state.[38] However, this has to be regarded with caution, since the final states of the transitions in a pair have to be the same in this interpretation. It also ignores the temperature dependence of the energies of the ground and excited states. It is thus clear that Δ' should be deduced more directly at a given temperature. As will be seen in the next section, Raman spectroscopy offers precisely such an opportunity.

V. LYMAN TRANSITIONS IN THE RAMAN EFFECT

A. Experimental observation

A transition which appears in the infrared as allowed by the electric-dipole selection rule may or may not manifest itself in the Raman spectrum requiring a nonvanishing polarizability. Indeed, in a system with a center of inversion in its point group symmetry, the rule of mutual exclusion states that a given transition can be observed either in the infrared or in the Raman effect but not in both.[43] To the extent the bound states of an acceptor in EMT are extended, the inversion symmetry is not broken and bound states continue to be of ''even'' or ''odd'' parity; in such a case, the $1s\rightarrow np$ transitions will appear in the infrared but be forbidden in the Raman effect. Conversely, the transitions between even parity states will be observed in the Raman effect but not in the infrared. Such selection rules will not be strict to the extent the ground and excited states are not effective-mass-like; however, T_d site symmetry must always prevail. Thus $1s\rightarrow 2s,3d,\ldots$ transitions might indeed be observed in the infrared, especially between states which have experienced significant central cell corrections.[44] In the context of these considerations, we explored the Raman spectrum of boron-doped diamond in the range extending from 0 to 3500 cm^{-1}. We have succeeded in observing the $1s(p_{3/2})\rightarrow 1s(p_{1/2})$ transition with a Raman shift of $\Delta'=16.7(1)$ cm^{-1} [16.2(1) cm^{-1}] for a natural (^{13}C) type IIb diamond at 5.0 K. The Raman cross sections for transitions to higher lying even parity states are significantly reduced and such transitions escape observation. The *absence* of the Δ' line in a spectrum recorded with type IIa specimens further confirmed the association of Δ' with boron acceptors. In the rest of the section, we discuss the Δ' line.

In Fig. 6(a), we show the Raman spectrum of a natural type IIb specimen (D1) recorded at 46 K in the right-angle scattering geometry: incident light along $x'||[110]$ and polarized along $z||[001]$; scattered light along $y'||[1\bar{1}0]$ but not analyzed. [In the notation of Damen, Porto, and Tell[45] this scattering configuration is labeled as $x'(zz+zx')y'$.] The observation of lines labeled Δ' both in the Stokes and

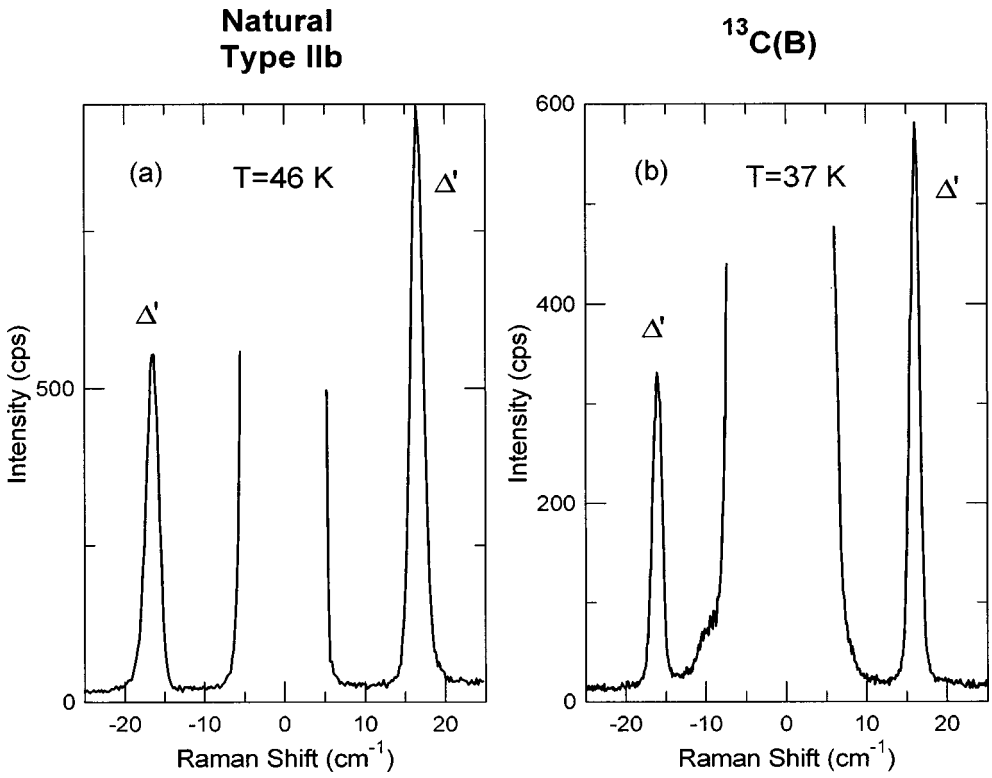

FIG. 6. The Stokes and anti-Stokes components of the $1s(p_{3/2})\rightarrow 1s(p_{1/2})$ Raman transition labeled Δ' in (a) a natural type IIb (D1) diamond at 46 K recorded in the right-angle scattering geometry $x'(zz+zx')y'$, $x'||[110]$, $y'||[1\bar{1}0]$, and $z||[001]$ and (b) a ^{13}C diamond at 37 K, in backscattering. Both spectra were excited with the 4765 Å Ar^+ laser line.

the anti-Stokes spectrum and their excitation with different laser lines[46] clearly established their Raman character. On the basis of similar observations, the lines labeled Δ' in Fig. 6(b) are the Stokes/anti-Stokes pair for a boron-doped ^{13}C diamond (D41), recorded at 37 K in backscattering.[47] Both spectra were excited with the 4765 Å line of an Ar^+ laser.

In Fig. 7, we display the temperature dependence of the Stokes component of Δ' in a man-made, boron-doped diamond of natural composition (D44). The spectra, excited with the 5309 Å line of a Kr^+ laser, are recorded in the backscattering geometry along [001]. The intensity of Δ' decreases and its width increases with increasing temperature. Above 200 K it finally becomes undetectable due to the combined effect of (1) thermal ionization of the boron acceptors and (2) line broadening, providing further evidence for its electronic nature.

B. Theoretical considerations

In this section we discuss the theoretical considerations underlying the polarization characteristics and the cross section of the Δ' line based on the interpretation that it arises from $1s(p_{3/2}):\Gamma_8$ to $1s(p_{1/2}):\Gamma_7$ transition. Noting that the reducible representation generated by the polarizability tensors $\Gamma(\alpha)=\Gamma_1+\Gamma_3+\Gamma_5$ and $\Gamma_8\times\Gamma_7=\Gamma_3+\Gamma_4+\Gamma_5$, only Γ_3 and Γ_5 polarizability tensors are relevant in this transition. Here we have used the nomenclature for $\bar{T}_d$, the double group appropriate for the T_d site symmetry of substitutional boron acceptors.[48] The relative importance of the Γ_3 and Γ_5 contributions is discussed below in the context of the Raman cross section of Δ'.

In a previous treatment[49] of electronic Raman scattering by shallow impurities in semiconductors, the cross section for Raman processes is obtained in the framework of the effective mass theory exploiting second-order $\mathbf{A}\cdot\mathbf{p}$ perturbation. In this theory the electron-photon interaction contains two terms, one linear in the vector potential $\mathbf{A}$ of the radiation field and the other quadratic in $\mathbf{A}$. We refer to the linear and quadratic terms as the paramagnetic and diamagnetic terms, respectively. In a Raman process, as in any two-photon process, one must consider in its lowest approximation the paramagnetic coupling in second order and the diamagnetic in first order. The ratio of the diamagnetic to the paramagnetic scattering amplitudes is of order $(\hbar\omega/E_I)$ where $\hbar\omega$ is the incident photon energy and E_I, a typical excitation energy of the impurity, e.g., its ionization energy.

It is also possible to express the scattering cross section in terms of an electron-photon coupling of the form $-\mathbf{d}\cdot\mathbf{E}$ where $\mathbf{d}$ is the electric-dipole moment of the system and $\mathbf{E}$ the electric field of the radiation. This approach has the advantage that the interaction between radiation and scattering system appears in first order only in the photon coordinates so that it is enough to take $-\mathbf{d}\cdot\mathbf{E}$ in second order. The two procedures are equivalent only in the long wavelength limit, i.e., when the wavelengths of the incident and scattered photons are long compared to the maximum diameter of the scattering system. The relation between these two methods has been discussed by several authors.[50] In the Appendix we give an outline of the relation between the $\mathbf{A}\cdot\mathbf{p}$ and $-\mathbf{d}\cdot\mathbf{E}$ approaches.

In the long wavelength approximation the differential scattering cross section for a Raman process in which a pho-

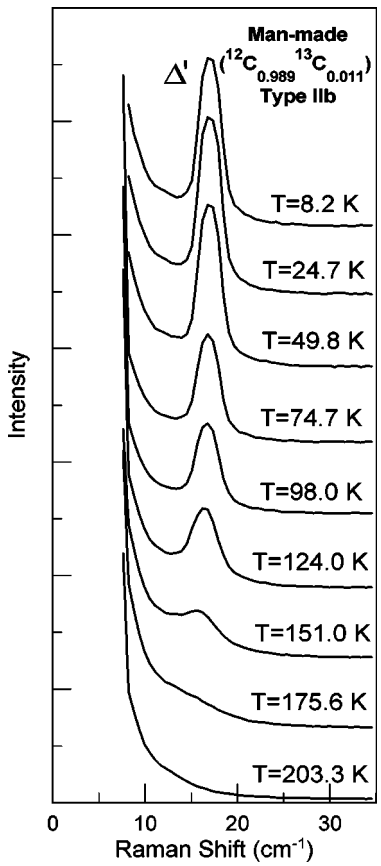

FIG. 7. The temperature dependence of the Δ' line in a man-made type IIb diamond with natural carbon composition. The spectra were excited with the 5309 Å Kr^+ laser line and recorded in backscattering ||[001].

ton of angular frequency ω and polarization along the unit vector $\hat{\boldsymbol{e}}$ is absorbed while one with frequency ω' and polarization $\hat{\boldsymbol{e}}'$ is emitted, with the scattering system experiencing a transition from $|\nu_0\rangle$ to $|\nu\rangle$, is

$$\frac{d\sigma}{d\Omega'}=\varepsilon_\infty^2\frac{(n'+1)\omega\omega'^3}{\hbar^2c^4}\times\left|\sum_{\nu'}\left(\frac{\hat{\boldsymbol{e}}'\cdot\mathbf{d}_{\nu\nu'}\hat{\boldsymbol{e}}\cdot\mathbf{d}_{\nu'\nu_0}}{\omega-\omega_{\nu'\nu_0}}-\frac{\hat{\boldsymbol{e}}\cdot\mathbf{d}_{\nu\nu'}\hat{\boldsymbol{e}}'\cdot\mathbf{d}_{\nu'\nu_0}}{\omega-\omega_{\nu\nu'}}\right)\right|^2. \tag{1}$$

Here $d\Omega'$ is an element of solid angle in the direction of propagation of the scattered photon; ε_∞ is the optical dielectric constant, which for the group IV elemental semiconductors is equal to ε_0, its static value, i.e., $\varepsilon_\infty=\varepsilon_0=n^2$, n being the refractive index, and

$$\hbar\omega_{\nu\nu'}=E_\nu-E_{\nu'}, \tag{2}$$

where E_ν is the energy eigenvalue of the Hamiltonian H_0 of the scattering system in the stationary state $|\nu\rangle$ and the sum over ν' extends over all intermediate states $|\nu'\rangle$. The symbol n' stands for the initial population of photons in the mode $(\omega',\hat{\boldsymbol{e}}')$; we shall assume from now on that $n'=0$. Furthermore we will be concerned with low-energy excitations $\omega_{\nu\nu_0}\ll\omega$ implying $\omega'\approx\omega$. The symbol $\mathbf{d}_{\nu\nu'}$ denotes the matrix element of the electric-dipole moment between $|\nu\rangle$ and $|\nu'\rangle$. Finally we stress that Eq. (1), valid only in the long wavelength approximation as already mentioned, is appropriate to the situations considered in this paper, viz., acceptors in the elemental semiconductors, in particular, diamond.

The stationary states of an acceptor are described in the effective mass approximation by wave functions of the form $|\nu\rangle=F_\nu(\mathbf{r})u(\mathbf{r})$, where $u(\mathbf{r})$ is a Bloch state at the center of the Brillouin zone, and $F_\nu(\mathbf{r})$ an envelope wave function satisfying the set of coupled differential equations

$$\left[\mathbf{D}(-i\boldsymbol{\nabla})-\frac{e^2}{\varepsilon_0 r}-\frac{2\Delta'}{3}\left(\mathbf{I}\cdot\mathbf{S}-\frac{1}{2}\right)\right]F_\nu(\mathbf{r})=E_\nu F_\nu(\mathbf{r}). \tag{3}$$

Here $\mathbf{D}(\mathbf{k})$ is a six-dimensional matrix whose components are differential operators; $F_\nu(\mathbf{r})$ is a six-component envelope wave function; and Δ' is the energy separation of the lowest levels of the acceptor resulting from spin-orbit interaction, i.e., the separation between the $1s(p_{3/2})$ and $1s(p_{1/2})$ states. $\mathbf{D}(\mathbf{k})$ is the direct product of the unit 2×2 matrix and

$$\mathbf{D}(\mathbf{k})=\sum_{i,j}\mathbf{D}_{ij}k_ik_j=\frac{\hbar^2}{m}\left[\frac{1}{2}\gamma_1k^2-3\gamma_2\sum_{i=1}^{3}k_i^2\left(I_i^2-\frac{1}{3}I^2\right)-3\gamma_3\sum_{i<j}k_ik_j\{I_i,I_j\}\right],\quad i,j=1,2,3 \tag{4}$$

where 1, 2, 3 refer to the cubic axes of the crystal, γ_1,γ_2, and γ_3 are the Luttinger parameters and I_1, I_2, and I_3 are the angular momentum matrices corresponding to angular momentum $I=1$. The expression in curly brackets is the anticommutator of the operators appearing in it.

The envelope function $F_\nu(\mathbf{r})$ varies slowly over the size of the primitive cell so that we can approximate the matrix elements of $\mathbf{d}$ as follows. Denoting by $\mathbf{n}$ a lattice position and by V_n the volume of the primitive cell at $\mathbf{n}$ we have

$$\langle\nu'|\mathbf{r}|\nu\rangle=\sum_n\int_{(V_n)}d\mathbf{r}\,F_{\nu'}^\dagger(\mathbf{r})u^\dagger(\mathbf{r})\mathbf{r}F_\nu(\mathbf{r})u(\mathbf{r})\approx\sum_n F_{\nu'}^\dagger(\mathbf{n})\mathbf{n}F_\nu(\mathbf{n})\int_{(V_0)}u^\dagger(\mathbf{r})u(\mathbf{r})d\mathbf{r}$$

after making use of the translational periodicity of $u(\mathbf{r})$. Taking $|\nu\rangle$ normalized to unity over the whole volume and $u(\mathbf{r})$ over the primitive cell,

$$\langle\nu'|\mathbf{r}|\nu\rangle\approx\int_{(V)}F_{\nu'}^\dagger(\mathbf{r})\mathbf{r}F_\nu(\mathbf{r})d\mathbf{r}.$$

For a hydrogenic center associated with a parabolic band, the matrix elements relevant to the calculation of the scattering cross section are those between the $1s$ ground state and the np excited states. The matrix elements $|\langle np|\mathbf{r}|1s\rangle|^2$ behave as n^{-3}, n being the principal quantum number of the intermediate $|np\rangle$ state. The sum over all excited p states, including the states in the continuum, is $3e^2a^2$ where a is the effective Bohr radius.[51] The total contribution to this sum due to the discrete states amounts to 72% of this total, so that

TABLE II. Wave functions for the Γ_8 and Γ_7 levels of an acceptor in its lowest-energy states. The convention $T|J,M\rangle = (-1)^{J-M}|J,-M\rangle$ is used for the action of the time reversal operator T.

$$\psi_{3/2} = -\frac{i}{\sqrt{2}}(\varepsilon_1 + i\varepsilon_2)\chi_+$$

$$\psi_{1/2} = -\frac{i}{\sqrt{6}}(\varepsilon_1 + i\varepsilon_2)\chi_- + i\sqrt{\frac{2}{3}}\varepsilon_3\chi_+$$

$$\phi_{1/2} = -\frac{i}{\sqrt{3}}(\varepsilon_1 + i\varepsilon_2)\chi_- - \frac{i}{\sqrt{3}}\varepsilon_3\chi_+$$

when $\hbar\omega \gg E_I$, it is legitimate to expand the quantities $(\omega - \omega_{\nu'\nu_0})^{-1}$ and $(\omega - \omega_{\nu\nu'})^{-1}$ in Eq. (1) in powers of ω^{-1}. These results should also hold for the acceptor states provided $\hbar\omega$ exceeds the ionization energy of the impurity.

The first term in the expansion of the quantity between the absolute value signs in Eq. (1) is exactly zero. The remaining terms are

$$\frac{1}{\omega^2}\sum_{\nu'}\left[\omega_{\nu'\nu_0}\hat{\boldsymbol{e}}'\cdot\mathbf{d}_{\nu\nu'}\hat{\boldsymbol{e}}\cdot\mathbf{d}_{\nu'\nu_0} - \omega_{\nu\nu'}\hat{\boldsymbol{e}}\cdot\mathbf{d}_{\nu\nu'}\hat{\boldsymbol{e}}'\cdot\mathbf{d}_{\nu'\nu_0}\right] + O\left(\frac{1}{\omega^3}\right). \tag{5}$$

We define a Hermitian operator K by

$$K = -i\left[\sum_{i,j}\mathbf{D}_{ij}k_ik_j, \hat{\boldsymbol{e}}\cdot\mathbf{d}\right] = -e\sum_{i,j}\mathbf{D}_{ij}(k_ie_j + k_je_i). \tag{6}$$

Using Eq. (6) it can be shown that the expression in Eq. (5) is

$$\begin{aligned}\frac{i}{\hbar\omega^2}\sum_{\nu'}&(\hat{\boldsymbol{e}}\cdot\mathbf{d}_{\nu\nu'}K_{\nu'\nu_0} - K_{\nu\nu'}\hat{\boldsymbol{e}}\cdot\mathbf{d}_{\nu'\nu_0}) + O\left(\frac{1}{\omega^3}\right)\\ &= \frac{i}{\hbar\omega^2}\langle\nu|[\hat{\boldsymbol{e}}'\cdot\mathbf{d}, K]|\nu_0\rangle + O\left(\frac{1}{\omega^3}\right)\\ &= \frac{e^2}{\hbar\omega^2}\left\langle\nu\left|\sum_{i,j}\mathbf{D}_{ij}(e_ie_j' + e_i'e_j)\right|\nu_0\right\rangle + O\left(\frac{1}{\omega^3}\right).\end{aligned} \tag{7}$$

Here we have used the fact that $\mathbf{d}$ commutes with the terms of the effective Hamiltonian in Eq. (3) not appearing in the definition of K. Substitution in Eq. (1) when $\omega_{\nu\nu_0} \ll \omega$ (i.e., $\omega' \approx \omega$) gives

$$\frac{d\sigma}{d\Omega'} \cong \varepsilon_\infty^2\left(\frac{e}{\hbar c}\right)^4\left|\left\langle\nu\left|\sum_{i,j}\mathbf{D}_{ij}(e_ie_j' + e_i'e_j)\right|\nu_0\right\rangle + O\left(\frac{1}{\omega}\right)\right|^2. \tag{8}$$

Neglecting terms in ω^{-1} in Eq. (8) is equivalent to disregarding the paramagnetic contributions to the scattering amplitude in the $\mathbf{A}\cdot\mathbf{p}$ approach. This result also explains why we do not observe Raman transitions to the higher ''even parity'' states of the acceptor. These would have an amplitude $E_I/\hbar\omega$ smaller than that of the $p_{3/2} \rightarrow p_{1/2}$ transition, and hence, its intensity would be $(E_I/\hbar\omega)^2$ smaller than that of the former. When $\hbar\omega \gg E_I$ the expansion in powers of ω^{-1} allows us to give a quantitative criterion for the validity of this result. Each term in the expansion of the scattering amplitude is smaller than that which precedes it by a factor at most of order $(E_I/\hbar\omega)$. Thus in the limit considered, the diamagnetic contribution to the scattering amplitude predominates over the paramagnetic.

TABLE III. Matrix elements $\langle\phi_m|\{I_i,I_j\}|\psi_M\rangle$ for $m = \frac{1}{2}, -\frac{1}{2}$ and $M = \frac{3}{2}, \frac{1}{2}, -\frac{1}{2}, -\frac{3}{2}$.

	m/M	$\frac{3}{2}$	$\frac{1}{2}$	$-\frac{1}{2}$	$-\frac{3}{2}$
$2I_3^2 - I_1^2 - I_2^2$	$\frac{1}{2}$	0	$\sqrt{2}$	0	0
	$-\frac{1}{2}$	0	0	$-\sqrt{2}$	0
$\sqrt{3}(I_1^2 - I_2^2)$	$\frac{1}{2}$	0	0	0	$\sqrt{2}$
	$-\frac{1}{2}$	$-\sqrt{2}$	0	0	0
$\{I_2,I_3\}$	$\frac{1}{2}$	$-i/\sqrt{6}$	0	$-i/\sqrt{2}$	0
	$-\frac{1}{2}$	0	$i/\sqrt{2}$	0	$i/\sqrt{6}$
$\{I_3,I_1\}$	$\frac{1}{2}$	$-1/\sqrt{6}$	0	$1/\sqrt{2}$	0
	$-\frac{1}{2}$	0	$1/\sqrt{2}$	0	$-1/\sqrt{6}$
$\{I_1,I_2\}$	$\frac{1}{2}$	0	0	0	$-i\sqrt{\frac{2}{3}}$
	$-\frac{1}{2}$	$-i\sqrt{\frac{2}{3}}$	0	0	0

The $p_{3/2}$ and $p_{1/2}$ states belong to the Γ_8 and Γ_7 irreducible representations of the double group $\overline{T}_d$ obtained from the reduction of $\Gamma_5 \times \Gamma_6$, the top of the p-like valence band transforming as Γ_5 and the spin of the hole as Γ_6. Denoting by $\varepsilon_1, \varepsilon_2, \varepsilon_3$ the Γ_5 states and by χ_+ and χ_- those belonging to Γ_6, the Γ_8 and Γ_7 states are given by the expressions in Table II. The Γ_5 states obey $I_1\varepsilon_1 = 0$, $I_1\varepsilon_2 = i\varepsilon_3$, $I_1\varepsilon_3 = -i\varepsilon_2$, with similar results for I_2 and I_3 obtained from these by cyclic permutation of the indices. The operator appearing in Eq. (8) can be decomposed into a sum of terms belonging to Γ_1, Γ_3, and Γ_5 as follows:

$$\begin{aligned}\sum_{i,j}\mathbf{D}_{ij}(e_ie_j' + e_i'e_j) = \frac{\hbar^2}{m}\Big[&\gamma_1\hat{\boldsymbol{e}}'\cdot\hat{\boldsymbol{e}} - \gamma_2\{(3I_3^2 - I^2)(3e_3'e_3\\ &- \hat{\boldsymbol{e}}'\cdot\hat{\boldsymbol{e}}) + 3(I_1^2 - I_2^2)(e_1'e_1 - e_2'e_2)\}\\ &- 3\gamma_3\sum_{i<j}\{I_i,I_j\}(e_i'e_j + e_ie_j')\Big].\end{aligned} \tag{9}$$

The matrix elements $\langle\phi_m|\{I_i,I_j\}|\psi_M\rangle$ between the Γ_8 states ψ_M $(M = \frac{3}{2}, \frac{1}{2}, -\frac{1}{2}, -\frac{3}{2})$ and the Γ_7 states ϕ_m $(m = \frac{1}{2}, -\frac{1}{2})$ are displayed in Table III. Finally, the cross sections for the $\psi_M \rightarrow \phi_m$ transitions are obtained from the amplitudes displayed in Table IV in the form

$$\frac{d\sigma}{d\Omega'} = \varepsilon_\infty^2\left(\frac{e^2}{mc^2}\right)^2|\hat{\boldsymbol{e}}'\cdot\boldsymbol{\alpha}\cdot\hat{\boldsymbol{e}}|^2. \tag{10}$$

The total differential scattering cross section for Raman transitions between Γ_8 and Γ_7 multiplets is

TABLE IV. The scattering amplitudes for the $\psi_M \rightarrow \phi_m$ Raman transitions. The differential cross sections are obtained using Eq. (10). Here we display the tensors $\boldsymbol{\alpha}$ (proportional to the electric polarizability) in terms of their components referred to the cubic axes.

$\psi_{\pm 3/2} \rightarrow \phi_{\pm 1/2}$	$\boldsymbol{\alpha} = \sqrt{\frac{3}{2}}\gamma_3 \begin{pmatrix} 0 & 0 & 1 \\ 0 & 0 & \pm i \\ 1 & \pm i & 0 \end{pmatrix}$
$\psi_{\pm 1/2} \rightarrow \phi_{\pm 1/2}$	$\boldsymbol{\alpha} = \mp\sqrt{2}\gamma_2 \begin{pmatrix} -1 & 0 & 0 \\ 0 & -1 & 0 \\ 0 & 0 & 2 \end{pmatrix}$
$\psi_{\pm 3/2} \rightarrow \phi_{\mp 1/2}$	$\boldsymbol{\alpha} = \sqrt{6} \begin{pmatrix} \pm\gamma_2 & i\gamma_3 & 0 \\ i\gamma_3 & \mp\gamma_2 & 0 \\ 0 & 0 & 0 \end{pmatrix}$
$\psi_{\pm 1/2} \rightarrow \phi_{\mp 1/2}$	$\boldsymbol{\alpha} = -\frac{3}{\sqrt{2}}\gamma_3 \begin{pmatrix} 0 & 0 & 1 \\ 0 & 0 & \pm i \\ 1 & \pm i & 0 \end{pmatrix}$

$$\frac{d\sigma}{d\Omega'} = \varepsilon_\infty^2 \left(\frac{e^2}{mc^2}\right)^2 \left[2\gamma_2^2 \left(3\sum_{i=1}^{3} e_i'^2 e_i^2 - (\hat{\boldsymbol{e}}' \cdot \hat{\boldsymbol{e}})^2 \right) + 3\gamma_3^2 \left(1 - 2\sum_{i=1}^{3} e_i'^2 e_i^2 + (\hat{\boldsymbol{e}}' \cdot \hat{\boldsymbol{e}})^2 \right) \right]. \quad (11)$$

The differential cross section for elastic scattering is

$$\frac{d\sigma}{d\Omega'} = \varepsilon_\infty^2 \left(\frac{e^2}{mc^2}\right)^2 \gamma_1^2 (\hat{\boldsymbol{e}}' \cdot \hat{\boldsymbol{e}})^2. \quad (12)$$

C. Comparison with experiments

In this section we present experimental results and interpret them on the basis of the above theoretical predictions. In Fig. 8 we display the Raman spectra measured for the natural type IIb diamond (D1) at 5.0 K, excited with the 4765 Å Ar^+ laser line and observed in backscattering along $z||[001]$. The incident light is polarized along $x'||[110]$ or $y'||[1\bar{1}0]$ and the scattered light analyzed along x' or y'. The polarization configurations yield the $(x'x')$, $(x'y')=(y'x')$, and $(y'y')$ components of the scattering tensor. Within the experimental limitations (mainly associated with the finite collection angle in the scattered beam), we conclude that the $(x'y')$ and $(y'x')$ components, even though allowed by symmetry, are negligible whereas the $(y'y')$ and the $(x'x')$ components are strong and equal in intensity. From Table IV we deduce the ratio of the scattering intensities for the $(x'y')$ and $(x'x')$ configuration to be $[\gamma_2^2/(\gamma_3^2+\frac{1}{3}\gamma_2^2)]$. The weak Δ' signature in the $(x'y')$ and $(y'x')$ polarizations in such experiments can well arise from the ''leakage'' of the strong $(x'x')$ and $(y'y')$ intensities. If the features in the $(x'y')$ and $(y'x')$ are considered genuine, one can conclude that $\gamma_2 \leqslant 0.1\gamma_3$. From their careful determination of the Hall coefficient factor of the holes in diamond, Reggiani, Waechter, and Zukotynski[52] deduce the mass parameters of the valence band or equivalently, the Luttinger parameters. In addition,

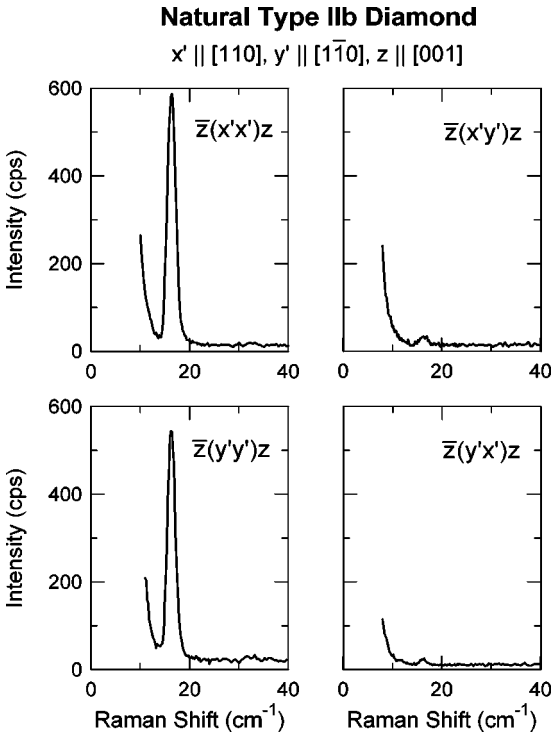

FIG. 8. The polarization features of the Δ' Raman line of a natural type IIb diamond in backscattering along $z||[001]$. The incident light is polarized along $x'||[110]$ or $y'||[1\bar{1}0]$ and the scattered light is analyzed along x' or y'. The spectra were excited with the 4765 Å line of an Ar^+ laser and recorded at 5.0 K.

their values are in excellent agreement with the theoretical calculations of van Haeringen and Junginger,[53] which gives $\gamma_2 \approx 0.085\gamma_3$, entirely consistent with our findings. *Thus we conclude that the* Δ' *Raman transition is predominantly* Γ_5 *in character.*

In order to determine the absolute Raman cross section of Δ', we have measured Δ', the Brillouin components, and the zone-center optical phonon of $\Gamma_5^+ \equiv F_{2g}$ symmetry at ω_0 in the *same* experiment with due regard to the effects of illumination and collection optics and grating efficiency. In Fig. 9 we present the spectrum of the natural type IIb diamond (D1) recorded in right-angle scattering geometry, $x'(zz+zx')y'$, at 5.0 K, where x', y', and z are defined in Fig. 6(a). Thus the scattering geometry selects the phonon wave vector to be along $[0\bar{1}0]$, generating the transverse acoustic (TA) and longitudinal acoustic (LA) Brillouin components. The relevant scattering cross sections in the scattering geometry used in Fig. 9 are

$$S_{\Delta'} = N_a \left(\frac{\varepsilon_\infty e^2}{mc^2}\right)^2 (3\gamma_3^2 + 4\gamma_2^2), \quad (13)$$

where N_a is the number of acceptors per unit volume,

$$S_{LA} = \varepsilon_\infty^6 \frac{\hbar(\omega_L - \omega_{LA})^4 \omega_{LA}}{32\pi^2 c^4 (1 - e^{-\hbar\omega_{LA}/kT})} \frac{p_{12}^2}{c_{11}}, \quad (14)$$

$$S_{TA} = \varepsilon_\infty^6 \frac{\hbar(\omega_L - \omega_{TA})^4 \omega_{TA}}{64\pi^2 c^4 (1 - e^{-\hbar\omega_{TA}/kT})} \frac{p_{44}^2}{c_{44}}, \quad (15)$$

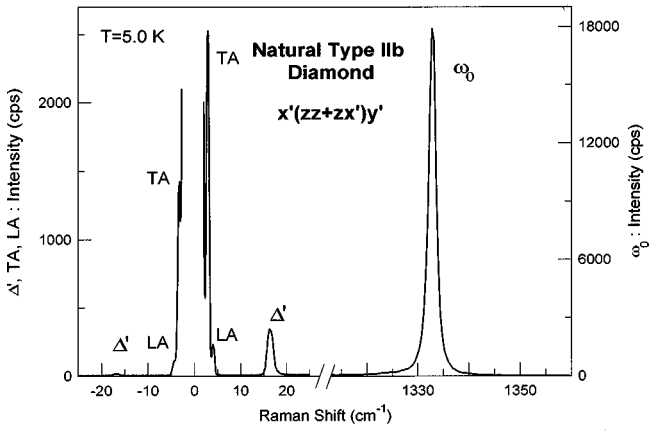

FIG. 9. Comparison of the intensities of the Brillouin components (TA and LA), the Δ' line, and the zone-center F_{2g} optical phonon at ω_0 in a natural type IIb diamond. The spectrum was recorded at 5.0 K in the $x'(zz+zx')y'$ geometry and excited with the 4765 Å line of an Ar^+ laser.

and

$$S_{\omega_0}=\frac{2\hbar(\omega_L-\omega_0)^4\varepsilon_\infty^2 N^2 s^2}{\rho c^4\omega_0(1-e^{-\hbar\omega_0/kT})}, \tag{16}$$

where ω_L, ω_{LA}, ω_{TA}, and ω_0 are the frequencies of the laser radiation, the LA, the TA, and the zone-center optical phonon, respectively; p_{12} and p_{44} are the elasto-optic constants; c_{12} and c_{44} are the elastic moduli; ρ is the density (3.512 g/cm^3); N is the number of primitive cells per unit volume ($=8.87\times10^{22}$/cm^3); s is the single independent component characterizing the Raman tensor per unit cell.

From the ratio $S_{\Delta'}$:S_{ω_0}, deduced from the areas of the Δ' and ω_0 line along with $|s|=4.4\pm0.3$ Å^2 (Ref. 54), $\gamma_2=0.09$ and $\gamma_3=1.06$ (Ref. 53), we obtain $N_a=(4.1\pm0.6)\times10^{16}$ cm^{-3}. This value is in good agreement with $(5.2\pm0.3)\times10^{16}$ cm^{-3} cited in Ref. 40 where the calibration is based on the strength of the Lyman transitions vs Hall coefficient.

Given the weak intensity of the Δ' line, we were forced to use a slit width which resulted in ''parasitic'' radiation of sufficient strength to appear in the spectral range of the Brillouin components observed in Fig. 9. While it is gratifying that the Brillouin components could be observed even at 5 K, their intensities could not be established with the confidence needed to calibrate the intensity of ω_0 and thus obtain $|s|$; we therefore used the value determined by Grimsditch and Ramdas.[54] (See also Ref. 55.) In order to obtain additional corroboration of $S_{\Delta'}$, we plan to measure the Brillouin components and the Δ' line using a multipassed tandem Fabry-Pérot interferometer with its superior rejection of parasitic radiation but with a free spectral range large enough to accommodate all the lines, on the other.

VI. DEFECT-INDUCED FIRST-ORDER SPECTRUM

As can be seen in Fig. 10, a quasicontinuous absorption band with a sharp feature labeled ω_0 appears in the spectra

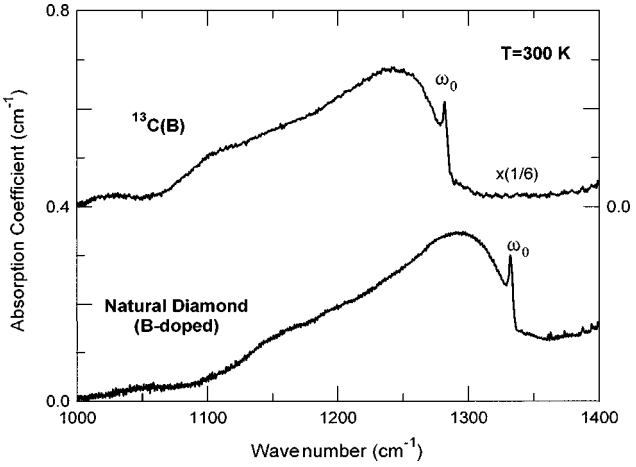

FIG. 10. Defect-induced-first-order (DIFO) spectra of type IIb ^{13}C and natural diamonds recorded at 300 K.

for both natural and ^{13}C boron-doped diamond in the frequency range of one-phonon excitations with wave vectors spanning the entire Brillouin zone. Though nominally forbidden by the requirement of wave vector conservation, the presence of boron acceptors presumably activates such vibrations due to a partial loss of translational symmetry. In the same spirit, the presence of ω_0, forbidden by dipole selection rule, can be attributed to the loss of center of inversion. The positions of ω_0 in the natural and the ^{13}C specimens are consistent with those from Raman measurements.[56] The spectrum for the ^{13}C diamond coincides with that for the natural diamond when the frequencies of the former are scaled by $(\bar{M}_{13}/\bar{M}_{\mathrm{nat}})^{1/2}$. The shift with isotopic composition is consistent with the prediction of the VCA.[57] We designate the one-phonon infrared spectrum activated by the boron acceptors in this manner as ''defect-induced-first-order'' spectrum. Note that the ω_0 feature occurs precisely at the infrared *inactive* but Raman *active* zone-center optical phonon observed in the Raman spectrum.

The DIFO spectrum (Fig. 11) measured at lower tempera-

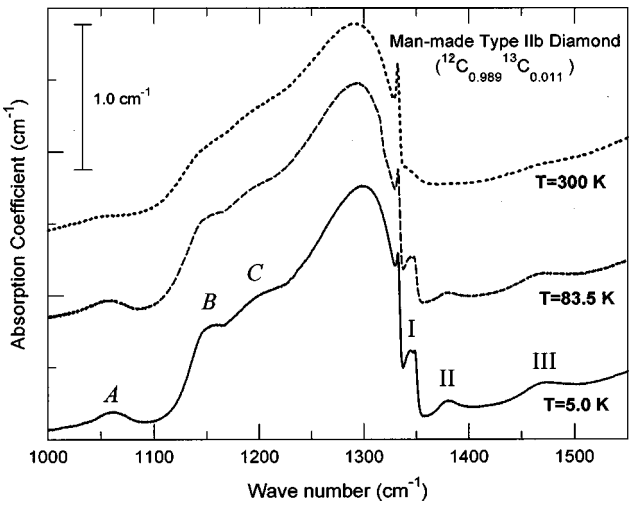

FIG. 11. DIFO feature as a function of temperature in a boron-doped man-made diamond with natural carbon composition. See text for the labels *A*, *B*, *C*, I, II, and III.

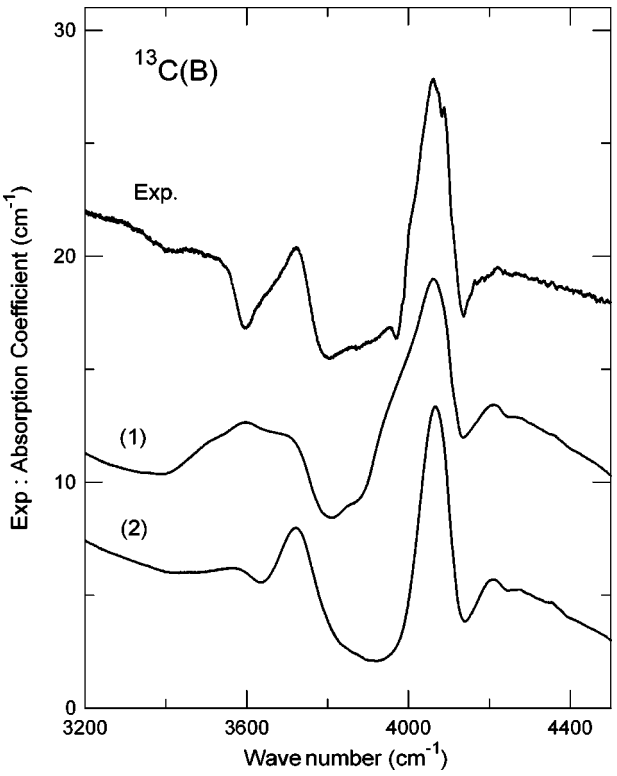

FIG. 12. Comparison of the experimental and computed (1,2) spectra of the ''DIFO plus acceptor excitations'' feature in boron-doped ^{13}C diamond in the range 3200–4500 cm^{-1}. For clarity, the computed spectra (1,2) are shifted vertically.

tures shows a general shift to higher frequencies, by ~ 6 cm^{-1} in going from 300 K to 5.0 K, with some features appearing more distinctly. The shift in ω_0 is comparatively less noticeable, consistent with the temperature dependence of the corresponding Raman line.[58] Three new features I, II, and III appear above ω_0 and shift with isotopic mass as $\bar{M}^{-1/2}$ along with the rest of the spectrum. It is of interest to note that I exhibits two closely spaced peaks, the one at the higher frequency occurring at an energy very close to that of $(\omega_0+\Delta')$. It is tempting to assign it to the simultaneous excitation of ω_0 and the $1s(p_{3/2})\rightarrow 1s(p_{1/2})$ transition. The interpretation for the broader features II and III is not clear at present.

In Fig. 12, we display the broad absorption peaks observed in ^{13}C type IIb diamond in the range 3200–4500 cm^{-1}. In the context of their energies one can interpret them as acceptor electronic transitions in combination with the DIFO of the ^{13}C diamond. The computed spectrum (1) is deduced by convoluting the DIFO with each of the electronic excitation lines in the range 2210–3500 cm^{-1}, after subtracting the contribution from the underlying multiphonon absorption. Features I, II, and III of Fig. 11 were omitted in the convolution process as being not relevant in the ''DIFO plus acceptor excitations.'' We also show (2) the results of such a convolution in which the broad peaks A, B, and C were excluded with suitable Voigt functions[59] to represent their contributions; the most prominent broad feature with its peak centered at 4063 cm^{-1} was interpreted as arising from two Voigt functions representing the DIFO in addition to ω_0. The success of such fits could be improved further with additional assumptions but it is not clear if they lead to new insights. As can be seen, both the computed spectra reproduce the observed experimental features satisfactorily but curve (2) succeeds in reproducing the shape of the strongest peak more convincingly. Similar computations for natural type IIb diamond also yielded a satisfactory representation for its DIFO plus acceptor excitations. Watkins and Fowler[60] have reported a sharp spectral feature in the excitation spectrum of boron acceptors in Si which they attributed to the ''ω_0 plus line 1'' combination, line 1 corresponding to the $\Gamma_8(1s_{3/2})\rightarrow\Gamma_8(2p_{3/2})$ transition;[61] the line shape of the peak shows the characteristic Fano interaction with the underlying continuum associated with the photoionization of the acceptors. We also note that, for Si(B), the zone-center optical phonon appears to be dominant in the DIFO. The strong continuum of the DIFO in diamond convoluted with the acceptor spectrum produces broad features overlapping the photoionization continuum; features recognizable as Fano interaction are presumably obliterated. Watkins and Fowler also draw attention to the puzzling absence of features associated with the higher acceptor excitations in combination with ω_0. However, Baron, Young, and McGill[62] succeeded in observing them in photoconductivity; the difference between absorption and photoconductivity spectra in this context has been emphasized by Chang and McGill.[63] Our interpretation for diamond, indeed, involves all the acceptor excitations.[64]

The above analysis of DIFO and DIFO plus electronic excitations clearly does not address some relevant issues: (1) What is the relationship of the shape of the DIFO spectrum to the one-phonon density of states? How does the manifestation of the density of states in the infrared spectrum get influenced by the dipole moment induced in the vibrations by the presence of boron acceptors?[14,65] Is the shape of such an ''activated'' spectrum impurity specific? (2) In the analogous case of diamonds with nitrogen impurities when four substitutional nitrogen atoms surround a vacancy (type IaB diamond), a one-phonon spectrum can indeed be observed along with the ω_0 line.[66] The possibility of an analogous situation in boron-doped diamond is unlikely in view of the growth conditions of the synthetic specimens. We also note here that the characteristics of the DIFO spectrum generated by the presence of boron impurities are distinct from those produced by nitrogen. (See Fig. 13.) (3) It is striking those the presence of boron in concentrations as low as 10^{16} cm^{-3} can produce an observable effect due to the partial loss of translation symmetry. (4) *Host-isotope-related shifts* in the local vibrational mode (LVM) frequencies of impurities have been noted for interstitial oxygen in Si and Ge.[67] Nitrogen interstitials also show evidence of nearest neighbor C's participating in the LVM; hence three signatures reflecting ^{12}C$-^{12}$C, ^{12}C$-^{13}$C, and ^{13}C$-^{13}$C have been observed.[68] It thus appears that DIFO-related spectrum of boron in $^{12}C_{1-x}{}^{13}C_x$ diamonds should be investigated for a range of x.

VII. CONCLUDING REMARKS

In the context of the departures from the effective mass theory of shallow donors and acceptors in the tetrahedrally coordinated elemental and compound semiconductors,[13,24] the present investigation has afforded a unique opportunity

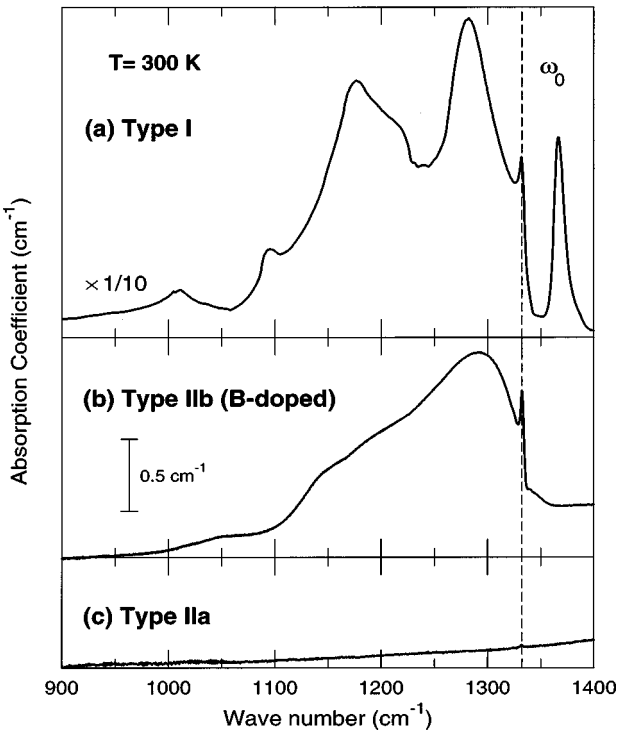

FIG. 13. The infrared absorption spectra of a natural type I, a man-made type IIb, and a natural type IIa diamond recorded at 300 K, compared in the spectral range of one-phonon frequencies, mainly those of the optical branches. The vertical scales in (b) and (c) are the same whereas that for (a) is compressed by a factor of 10. The vertical line is located at $\omega_0 = 1332.4\ \mathrm{cm}^{-1}$, the frequency of the Raman line at 300 K.

of exposing host-isotope-related self-energy shifts in the energy levels. As emphasized in the present paper, the binding energies of both the ground and excited states of holes bound to boron acceptors in diamond experience shifts as the isotopic composition of the host is changed from natural to ^{13}C. In Si and Ge, the evidence for the departure from the effective mass theory is unmistakable for the ground states of donors as well as acceptors. The Lyman spectra of the group V donors in Si and Ge exhibit the *same spacing* between corresponding lines, on one hand, but the entire spectrum of one impurity is displaced with respect to those of the others, on the other hand. This behavior is also displayed by the group III acceptors in Ge and, to a lesser extent, in Si. These observations have led to a large number of studies addressing the so-called ''chemical'' shifts of the ground states in the different acceptors and the ''valley-orbit splitting'' of the ground state of donors in a semiconductor with multivalley conduction band. At the present, deliberate doping in diamond has been possible only with substitutional boron; a knowledge of the chemical shifts and valley-orbit splittings in the case of diamond will have to await corresponding successes in doping of diamond. Noting that the dielectric constant of the diamond is ~ 6, in contrast to ~ 12 and ~ 16 for Si and Ge, respectively, it is not surprising that central cell correction will continue to manifest even for highly excited states of acceptors in diamond; the complexity of the Lyman spectrum of boron in diamond is apparently due to the significantly higher binding energies and the smaller ''Bohr radii'' associated with this feature. Self-energy effects in relation to the central cell corrections can obviously be fully addressed only after a number of the group III acceptors are successfully incorporated in isotopically controlled diamonds.

The spin-orbit splitting of the acceptor ground state, Δ', is clearly correlated with the separation, Δ, between the $p_{3/2}$ and the $p_{1/2}$ valence bands. Thus it is reasonable that the Δ' obtained in our measurements [in the Lyman spectra through the thermal population of the $p_{1/2}(\Gamma_7)$ ground state as well as more directly as a Raman transition between $1s(p_{3/2}) \rightarrow 1s(p_{1/2})$ levels] is only $\Delta' = 2.07$ meV for natural diamond to be compared with $\Delta \sim 6$ meV.[36] Wright and Mooradian[69] observed the Δ' Raman line in Si at 23.4 meV for boron acceptors, Δ being ~ 44 meV.[61] From the study of stress and Zeeman splitting of this electronic Raman line, Cherlow, Aggarwal, and Lax[70] determined the deformation potentials and g values of the boron acceptor ground states. Our preliminary observations, indeed, show the splitting of the Δ' line into two components under applied uniaxial stress which splits the fourfold degenerate $1s(p_{3/2})$ into two states without affecting the double degeneracy of the $1s(p_{1/2})$ state.[61] Our recent experiments show that, in the presence of an applied magnetic field, the spin degeneracies of both $1s(p_{3/2})$ and $1s(p_{1/2})$ states are lifted and the Δ' line exhibits splittings with a somewhat more complex pattern. Both piezospectroscopy and magnetospectroscopy of the Δ' transition are being actively investigated currently and the results will be reported in a separate publication. Chandrasekhar, Ramdas, and Rodriguez[71] observed the Δ' line of Si(B) in the infrared at 22.77 meV, but our attempt to detect the Δ' line in boron-doped diamond in infrared was unsuccessful, presumably due to low acceptor concentration. Doehler, Colwell, and Solin[72] who studied the electronic Raman effect of Ge(Ga), did not report the Δ' line; the large spin-orbit splitting (~ 290 meV) presumably results in the overlap of the $1s(p_{1/2})$ level with the $p_{3/2}$ continuum and hence a significant broadening may have militated against the observation of the Δ' line.

In addition to the Lyman and Raman spectroscopy of the boron acceptors in diamond presented in this paper, we draw attention to the recent investigations of Sharp *et al.*,[73] Sternschulte *et al.*,[74] and Ruf *et al.*[75] Exploiting cathodoluminescence, they have observed luminescence associated with excitons bound to neutral boron acceptors. Part of the fine structure in their spectra arises from the Δ' splitting of the boron ground state; it is gratifying to note that they obtain $\Delta' = 2 \pm 0.2$ meV.

ACKNOWLEDGMENTS

The authors acknowledge support from the National Science Foundation Grant No. DMR 93-03186 at Purdue and from the U.S. Department of Energy, BES Material Sciences (Grant No. W-31-109-ENG-38) at Argonne National Laboratory. Thanks are also due to G. C. La Rocca, F. Bassani, and R. Collela for useful discussions and advice. S. R. thanks Scuola Normale Superiore for the hospitality extended during a part of the work.

APPENDIX

In order to demonstrate the equivalence of the $\mathbf{A}\cdot\mathbf{p}$ and $-\mathbf{d}\cdot\mathbf{E}$ approaches for treating electron-photon interactions

in the long wavelength limit, we consider a system of N charged particles with charges q_i and masses m_i ($i=1,2,\ldots,N$) in interaction with an electromagnetic field described by the vector potential

$$\mathbf{A}(\mathbf{r})=\sum_{q\mu}\left(\frac{2\pi\hbar c^2}{V\omega_q}\right)^{1/2}\hat{\boldsymbol{e}}_{q\mu}(a_{q\mu}+a_{q\mu}^{\dagger}), \tag{A1}$$

where the factors $\exp(\pm i\mathbf{q}\cdot\mathbf{r})$ have been set equal to unity in the long wavelength approximation. Here ω_q and $\hat{\boldsymbol{e}}_{q\mu}$ are the angular frequency and unit polarization vector of a photon of wave vector $\mathbf{q}$, μ being the label of one of the two possible orthogonal directions of polarization. The operators $a_{q\mu}$ and $a_{q\mu}^{\dagger}$ are destruction and creation operators for photons characterized by $\mathbf{q}$ and μ. We take the origin of the coordinates within the system of interest and V is the volume of quantization of the radiation field. The Hamiltonian of the system in the absence of the radiation is denoted by H_0 and consists of the kinetic energy of all the particles and their mutual interactions described neglecting retardation, since we assume the system to be confined within a volume whose maximum diameter is small compared with the wavelength of the radiation. The Hamiltonian of the system is

$$H=\sum_{i=1}^{N}\frac{1}{2m_i}\left(\mathbf{p}_i-\frac{q_i}{c}\mathbf{A}\right)^2+U(\mathbf{r}_1,\mathbf{r}_2,\ldots,\mathbf{r}_N)+\sum_{q\mu}\hbar\omega_q\left(a_{q\mu}^{\dagger}a_{q\mu}+\frac{1}{2}\right), \tag{A2}$$

and the eigenstates of H_0 are denoted by $|\nu\rangle$:

$$H_0|\nu\rangle=E_\nu|\nu\rangle. \tag{A3}$$

We now perform a canonical transformation defined by

$$\tilde{H}=\exp\left(-\frac{i}{\hbar c}\mathbf{d}\cdot\mathbf{A}\right)H\exp\left(\frac{i}{\hbar c}\mathbf{d}\cdot\mathbf{A}\right), \tag{A4}$$

where $\mathbf{d}=\Sigma_i^N q_i\mathbf{r}_i$ is the electric-dipole moment of the system of charged particles. We obtain

$$\tilde{H}=\sum_{i=1}^{N}\frac{p_i^2}{2m_i}+U(\mathbf{r}_1,\mathbf{r}_2,\ldots,\mathbf{r}_N)+\sum_{q\mu}\hbar\omega_q\left(a_{q\mu}^{\dagger}a_{q\mu}+\frac{1}{2}\right)-\mathbf{d}\cdot\mathbf{E}+\sum_{q\mu}\frac{2\pi}{V}(\mathbf{d}\cdot\hat{\boldsymbol{e}}_{q\mu})^2. \tag{A5}$$

The last term in $\tilde{H}$ is an electric-dipole self-energy which does not contain the photon coordinates. The sums over $q\mu$ should be restricted to the long wavelength photons under consideration. The states of $\tilde{H}_0$ are of the form $\exp(-i\mathbf{d}\cdot\mathbf{A}/\hbar c)|\nu\rangle=|\tilde{\nu}\rangle$ and $\tilde{H}_0|\tilde{\nu}\rangle=E_\nu|\tilde{\nu}\rangle$. Standard second-order perturbation theory using the form (A5) of the Hamiltonian leads to the result quoted in Eq. (1). In addition, since the $\exp(-i\mathbf{d}\cdot\mathbf{A}/\hbar c)$ and $\mathbf{d}$ commute,

$$\langle\tilde{\nu}'|\mathbf{d}|\tilde{\nu}\rangle=\langle\nu'|\mathbf{d}|\nu\rangle=\mathbf{d}_{\nu'\nu}. \tag{A6}$$

[1] R. Robertson, J. J. Fox, and A. E. Martin, Philos. Trans. R. Soc. London, Ser. A **232**, 463 (1934).

[2] M. Lax and E. Burstein, Phys. Rev. **97**, 39 (1955).

[3] W. Kaiser and W. L. Bond, Phys. Rev. **115**, 857 (1959).

[4] J. F. H. Custers, Physica (Amsterdam) **18**, 489 (1952); **20**, 183 (1954). Resistivities as low as 5 Ω cm have since been encountered.

[5] I. G. Austin and R. Wolfe, Proc. Phys. Soc. London, Sect. B **69**, 329 (1956).

[6] P. T. Wedepohl, Proc. Phys. Soc. London, Sect. B **70**, 177 (1957).

[7] J. J. Charette, Physica (Amsterdam) **27**, 1061 (1961).

[8] S. D. Smith and W. Taylor, Proc. Phys. Soc. London **79**, 1142 (1962).

[9] J. R. Hardy, S. D. Smith, and W. Taylor, *The Physics of Semiconductors* (The Institute of Physics and Physical Society, London, 1962), p. 521.

[10] T. R. Anthony and W. F. Banholzer, Diamond Relat. Mater. **1**, 717 (1992).

[11] J. C. Angus and C. C. Hayman, Science **241**, 913 (1988).

[12] See A. T. Collins and A. W. S. Williams, J. Phys. C **4**, 1789 (1971); R. M. Chrenko, Phys. Rev. B **7**, 4560 (1973); E. C. Lightowlers and A. T. Collins, J. Phys. D **9**, 951 (1976). On the basis of a critical examination of the literature and their own investigations these authors concluded that the ''acceptor'' in semiconducting diamond is substitutional boron.

[13] A. K. Ramdas and S. Rodriguez, Rep. Prog. Phys. **44**, 1297 (1981).

[14] H. Kim, A. K. Ramdas, S. Rodriguez, and T. R. Anthony, Solid State Commun. **102**, 861 (1997).

[15] H. Kim, R. Vogelgesang, A. K. Ramdas, S. Rodriguez, M. Grimsditch, and T. R. Anthony, Phys. Rev. Lett. **79**, 1706 (1997). In the figure caption for Fig. 2(b) the scattering configuration should read $x'(zz+zx')y'$.

[16] Aldrich Chemical Company, 1001 West Saint Paul Ave., Milwaukee, WI 53233.

[17] BOMEM, Inc., 450 St-Jean Baptiste Ave., Quebec, Quebec G2E 5S5, Canada.

[18] Graseby Infrared, 12151 Research Parkway, Orlando, FL 32826.

[19] Instruments S.A., Inc., Jobin Yvon/Spex Division, 3880 Park Avenue, Edison, NJ 08820.

[20] Coherent, Inc., Laser Group, 5100 Patrick Henry Drive, Santa Clara, CA 95054.

[21] Spectra-Physics Lasers, Inc., 1335 Terra Bella Avenue, P.O. Box 7013, Mountain View, CA 94043.

[22] Omnichrome, 13580 5th St., Chino, CA 91710.

[23] Janis Research Company, Inc., 2 Jewel Drive, Wilmington, MA 01887.

[24] W. Kohn, in *Solid State Physics: Advances in Research and Applications*, edited by F. Seitz and D. Turnbull (Academic, New York, 1957), Vol. 5, p. 257.

[25] J. M. Luttinger, Phys. Rev. **102**, 1030 (1956). The relation of the Luttinger parameters to others used in the literature are $A=-(\hbar^2\gamma_1/2m)$, $B=-(\hbar^2\gamma_2/m)$, $D=-(\sqrt{3}\hbar^2\gamma_3/m)$, and $L=A+2B$, $M=A-B$, $N=D\sqrt{3}$. We use the form of $\mathbf{D}$ as given in Ref. 13.

[26] S. T. Pantelides, Rev. Mod. Phys. **50**, 797 (1978).
[27] G. Davies and R. Stedman, J. Phys. C **20**, 2119 (1987).
[28] A. T. Collins and E. C. Lightowlers, Phys. Rev. **171**, 843 (1968).
[29] Even though there is no inversion symmetry, the wave functions have definite parity with a high degree of approximation.
[30] F. Bassani and A. Quattropani, Solid State Commun. **53**, 1077 (1985); N. Binggeli, A. Baldereschi, and A. Quattropani, in *Shallow Impurities in Semiconductors 1988*, edited by B. Monemar, IOP Conf. Proc. No. 95 (Institute of Physics and Physical Society, Bristol, England, 1989), p. 521.
[31] J. W. Nibler and G. V. Knighten, in *Raman Spectroscopy of Gases and Liquids*, edited by A. Weber (Springer, Berlin, 1979), p. 253.
[32] P. J. Dean, J. D. Cuthbert, D. G. Thomas, and R. T. Lynch, Phys. Rev. Lett. **18**, 122 (1967).
[33] A. E. Mayer and E. C. Lightowlers, J. Phys. C **13**, L747 (1980).
[34] D. Labrie, T. Timusk, and M. L. W. Thewalt, Phys. Rev. Lett. **52**, 81 (1984).
[35] R. A. Street and W. Senske, Phys. Rev. Lett. **37**, 1292 (1976).
[36] C. J. Rauch, Phys. Rev. Lett. **7**, 83 (1961); *The Physics of Semiconductors* (The Institute of Physics and Physical Society, London, 1962), p. 276.
[37] N. O. Lipari and A. Baldereschi, Solid State Commun. **25**, 665 (1978).
[38] P. A. Crowther, P. J. Dean, and W. F. Sherman, Phys. Rev. **154**, 772 (1967).
[39] E. Anastassakis, Phys. Rev. **186**, 760 (1969).
[40] See A. T. Collins and A. W. S. Williams, J. Phys. C **4**, 1789 (1971). Using their calibration curve for neutral acceptor concentration, the boron concentration in our type IIb diamond samples is estimated to be $(1.7\pm0.1)\times10^{16}$ cm^{-3} for D2, $(5.2\pm0.3)\times10^{16}$ cm^{-3} for D1, $(2.6\pm0.1)\times10^{17}$ cm^{-3} for D44 (a man-made diamond of natural composition), and $(2.8\pm0.1)\times10^{17}$ cm^{-3} for D41 (^{13}C, boron-doped diamond).
[41] M. Cardona (private communication).
[42] A. T. Collins, S. C. Lawson, G. Davies, and H. Kanda, Phys. Rev. Lett. **65**, 891 (1990).
[43] G. Herzberg, *Molecular Spectra and Molecular Structure, II. Infrared and Raman Spectra of Polyatomic Molecules* (D. Van Nostrand Company, Inc., Princeton, NJ, 1945), p. 256.
[44] W. H. Kleiner and W. E. Krag, Phys. Rev. Lett. **25**, 1490 (1970).
[45] Following T. C. Damen, S. P. S. Porto, and B. Tell, Phys. Rev. **142**, 570 (1966), we denote the scattering geometry by $i(jk)l$, where i is the incident direction, j the incident polarization, k the scattered polarization, and l the scattered direction.
[46] The Raman spectrum was excited with 4131, 4762, 4825, 5309, and 6471 Å lines of a Kr^+ laser; 4416 Å line of a He-Cd laser; and 4579, 4765, 4880, and 5145 Å lines of an Ar^+ laser.
[47] Our boron-doped ^{13}C diamond is a platelet (2 mm diameter, 0.35 mm thick) with its normal close to [001].
[48] G. F. Koster, J. O. Dimmock, R. G. Wheeler, and H. Statz, *Properties of the Thirty-two Point Groups* (MIT Press, Cambridge, MA, 1963).
[49] M. V. Klein, in *Light Scattering in Solids*, edited by M. Cardona (Springer, Heidelberg, 1975), p. 147.
[50] See, for example, C. Cohen-Tannoudji, J. Dupont-Roc, and G. Grynberg, *Photons and Atoms, Introduction to Quantum Electrodynamics* (Wiley, New York, 1989), Chap. IV, especially complement B_{IV}.
[51] H. A. Bethe and E. E. Salpeter, *Quantum Mechanics of One- and Two-Electron Atoms* (Academic, New York, 1957).
[52] L. Reggiani, D. Waechter, and S. Zukotynski, Phys. Rev. B **28**, 3550 (1983).
[53] W. van Haeringen and H. -G. Junginger, Solid State Commun. **7**, 1135 (1969). Based on the discussion in Ref. 52, we use $|\gamma_1|=3.61$, $|\gamma_2|=0.09$, and $|\gamma_3|=1.06$ for diamond.
[54] M. H. Grimsditch and A. K. Ramdas, Phys. Rev. B **11**, 3139 (1975).
[55] M. Grimsditch, M. Cardona, J. M. Calleja, and F. Meseguer, J. Raman Spectrosc. **10**, 77 (1981).
[56] R. Vogelgesang, A. K. Ramdas, S. Rodriguez, M. Grimsditch, and T. R. Anthony, Phys. Rev. B **54**, 3989 (1996).
[57] See, for example, K. C. Hass, M. A. Tamor, T. R. Anthony, and W. F. Banholzer, Phys. Rev. B **45**, 7171 (1992).
[58] S. A. Solin and A. K. Ramdas, Phys. Rev. B **1**, 1687 (1970).
[59] B. Di Bartolo, *Optical Interactions in Solids* (Wiley, Inc., New York, 1968), Chap. 15.
[60] G. D. Watkins and W. B. Fowler, Phys. Rev. B **16**, 4524 (1977).
[61] A. Onton, P. Fisher, and A. K. Ramdas, Phys. Rev. **163**, 686 (1967).
[62] R. Baron, M. H. Young, and T. C. McGill, Solid State Commun. **47**, 167 (1983).
[63] Y. C. Chang and T. C. McGill, Solid State Commun. **47**, 171 (1983).
[64] The authors of Ref. 27 interpret the feature peaked at 508 meV as a one-phonon sideband of the strongest electronic excitation (346 meV), the phonon having the mean energy of optical phonon band; further, they attribute the line shape to a Fano interaction. On the basis of Fig. 12, our interpretation appears more realistic.
[65] J. F. Angress, S. D. Smith, and K. F. Renk, in *Lattice Dynamics*, edited by R. F. Wallis (Pergamon, London, UK, 1965).
[66] G. Davies, in *Chemistry and Physics of Carbon*, edited by P. L. Walker, Jr. and P. A. Thrower (Marcel Dekker, Inc., New York, 1977), Vol. 13, p. 1. See also J. H. N. Loubser and J. A. van Wyk quoted by C. D. Clark *et al.*, in *The Properties of Natural and Synthetic Diamond*, edited by J. E. Field (Academic, London, 1992), p. 35.
[67] A. J. Mayur, M. Dean Sciacca, M. K. Udo, A. K. Ramdas, K. Itoh, J. Wolk, and E. E. Haller, Phys. Rev. B **49**, 16 293 (1994).
[68] I. Kiflawi, A. Mainwood, H. Kanda, and D. Fisher, Phys. Rev. B **54**, 16 719 (1996).
[69] G. B. Wright and A. Mooradian, Phys. Rev. Lett. **18**, 608 (1967).
[70] J. M. Cherlow, R. L. Aggarwal, and B. Lax, Phys. Rev. B **7**, 4547 (1973).
[71] H. R. Chandrasekhar, A. K. Ramdas, and S. Rodriguez, Phys. Rev. B **12**, 5780 (1975).
[72] J. Doehler, P. J. Colwell, and S. A. Solin, Phys. Rev. B **9**, 636 (1974).
[73] S. J. Sharp, A. T. Collins, G. Davies, and G. S. Joyce, J. Phys.: Condens. Matter **9**, L451 (1997).
[74] H. Sternschulte, S. Wahl, K. Thonke, R. Sauer, T. Ruf, M. Cardona, and T. R. Anthony, Mater. Sci. Forum **258-263**, 757 (1997).
[75] T. Ruf, M. Cardona, H. Sternschulte, S. Wahl, K. Thonke, R. Sauer, P. Pavone, and T. R. Anthony, Solid State Commun. **105**, 311 (1998).